Systems/Circuits

MIF versus SIF Motoneurons, What Are Their Respective Contribution in the Oculomotor Medial Rectus Pool?

Génova Carrero-Rojas,[1,2*] Rosendo G. Hernández,[1*] Roland Blumer,[2] Rosa R. de la Cruz,[1#] and Angel M. Pastor[1#]
[1]Departamento de Fisiología, Facultad de Biología, Universidad de Sevilla, Seville 41012, Spain, and [2]Center of Anatomy and Cell Biology, Medical Imaging Cluster, Medical University Vienna, Vienna 1090, Austria

Multiply-innervated muscle fibers (MIFs) are peculiar to the extraocular muscles as they are non-twitch but produce a slow build up in tension on repetitive stimulation. The motoneurons innervating MIFs establish en grappe terminals along the entire length of the fiber, instead of the typical en plaque terminals that singly-innervated muscle fibers (SIFs) motoneurons establish around the muscle belly. MIF motoneurons have been proposed to participate only in gaze holding and slow eye movements. We aimed to discern the function of MIF motoneurons by recording medial rectus motoneurons of the oculomotor nucleus. Single-unit recordings in awake cats demonstrated that electrophysiologically-identified medial rectus MIF motoneurons participated in different types of eye movements, including fixations, rapid eye movements or saccades, convergences, and the slow and fast phases of the vestibulo-ocular nystagmus, the same as SIF motoneurons did. However, MIF medial rectus motoneurons presented lower firing frequencies, were recruited earlier and showed lower eye position (EP) and eye velocity (EV) sensitivities than SIF motoneurons. MIF medial rectus motoneurons were also smaller, had longer antidromic latencies and a lower synaptic coverage than SIF motoneurons. Peristimulus time histograms (PSTHs) revealed that electrical stimulation to the myotendinous junction, where palisade endings are located, did not recurrently affect the firing probability of medial rectus motoneurons. Therefore, we conclude there is no division of labor between MIF and SIF motoneurons based on the type of eye movement they subserve.

Key words: **eye movements; motoneuron; multiply innervated fiber; oculomotor system; palisade endings; singly innervated fiber**

Significance Statement

In addition to the common singly-innervated muscle fiber (SIF), extraocular muscles also contain multiply-innervated muscle fibers (MIFs), which are non-twitch and slow in contraction. MIF motoneurons have been proposed to participate only in gaze holding and slow eye movements. In the present work, by single-unit extracellular recordings in awake cats, we demonstrate, however, that both SIF and MIF motoneurons, electrophysiologically-identified, participate in the different types of eye movements. However, MIF motoneurons showed lower firing rates (FRs), recruitment thresholds, and eye-related sensitivities, and could thus contribute to the fine adjustment of eye movements. Electrical stimulation of the myotendinous junction activates antidromically MIF motoneurons but neither MIF nor SIF motoneurons receive a synaptic reafferentation that modifies their discharge probability.

Received July 20, 2021; revised Aug. 18, 2021; accepted Oct. 11, 2021.

Author contributions: G.C.-R., R.G.H., R.R.d.l.C., and A.M.P. performed research; G.C.-R., R.G.H., and R.B. analyzed data; G.C.-R., R.G.H., R.R.d.l.C., R.B., and A.M.P. edited the paper; R.R.d.l.C., R.B., and A.M.P. designed research; R.R.d.l.C. wrote the first draft of the paper; R.R.d.l.C. and A.M.P. wrote the paper.

This paper is part of the I+D+i project PGC2018-094654-B-100 supported by MCIN/ AEI/10.13039/501100011033, FEDER "A way of making Europe". Also supported by Austrian Science Fund, Grant P32463-B and FIUS project PRJ202104162. RGH was a Postdoctoral fellow funded by Junta de Andaluía and European Social Fund. Confocal microscopy was performed at the Central Research Services of the Universidad de Sevilla (CITIUS).

*G.C.-R. and R.G.H are co-first authors.

#R.R.d.l.C. and A.M.P. are co-senior authors.

The authors declare no competing financial interests.

Correspondence should be addressed to Angel M. Pastor at ampastor@us.es.

https://doi.org/10.1523/JNEUROSCI.1480-21.2021

Introduction

Multiply-innervated muscle fibers (MIFs) of mammals show remarkably different structural and functional characteristics as compared with the canonical singly-innervated muscle fibers (SIFs). MIFs are only found in extraocular, laryngeal, and middle inner ear muscles (Schiaffino and Reggiani, 2011). MIFs are small fibers with a poorly developed sarcoplasmic reticulum which do not respond on electrical stimulation with a twitch-like tension, rather a graded slow and small-amplitude contraction on repetitive stimulation, and are also known as slow or non-twitch fibers (Bach-y-Rita and Ito, 1966; Pilar, 1967; Shall and Goldberg, 1992). The motoneuronal innervation of MIFs is also unusual since they receive multiple en grappe synaptic terminals

along their length arising from thin axons (Hess and Pilar, 1963; Namba et al., 1968; Mayr, 1971; Bondi and Chiarandini, 1983). In contrast, SIFs are large-size muscle fibers innervated by large-diameter motoneuronal axons forming the classical en plaque neuromuscular junction (Namba et al., 1968; Mayr, 1971), as in the skeletal musculature, and generating a twitch on stimulation.

The physiological role of MIF motoneurons is intriguing due, in part, to the peculiarities of the muscle fibers they innervate. It has been suggested that they could contribute differentially to the generation of eye movements, compared with SIF motoneurons (Büttner-Ennever and Horn, 2002; Wasicky et al., 2004; Eberhorn et al., 2006; Ugolini et al., 2006). Thus, MIF motoneurons might participate in gaze holding and slow eye movements, whereas SIF motoneurons would participate in all types of eye movements. Two types of experiments have led to this suggestion. First, morphologic studies have demonstrated that MIF motoneurons are mainly located at the periphery of the oculomotor nuclei, anatomically segregated from SIF motoneurons. This has been shown in humans (Horn et al., 2018), monkeys (Büttner-Ennever et al., 2001; Wasicky et al., 2004; Büttner-Ennever, 2006; Erichsen et al., 2014; Tang et al., 2015), rats (Eberhorn et al., 2006), and in the medial rectus subgroup of the oculomotor nucleus in cats (Bohlen et al., 2017b). Nevertheless, in the cat abducens nucleus, MIF and SIF motoneurons have been found intermingled (Hernández et al., 2019). Second, anatomic studies of the afferent inputs to MIF and SIF motoneurons have revealed that these two types of motoneuron receive, in general, different projections. Thus, in primates, the anterograde labeling of afferents to oculomotor MIF and SIF motoneurons (Wasicky et al., 2004) and the retrograde transneuronal tracing of rabies virus injected into the distal portion of the lateral rectus muscle (where en grappe terminals of MIF motoneurons are located) have shown a differential innervation pattern of MIF and SIF motoneurons, so that "tonic" inputs, those responsible for a sustained firing during fixations such as vestibular and prepositus hippoglossi neurons, terminate on MIF motoneurons, which virtually do not receive "fast" afferents (i.e., burst reticular neurons), whereas SIF motoneurons receive all known types of preoculomotor, "slow" and "fast," afferents (Ugolini et al., 2006).

It is also important to highlight that MIF, but not SIF motoneurons, in addition to the en grappe terminals along the muscle fiber, give rise to the so-called palisade endings at the myotendinous junction, which are particularly abundant in the medial rectus muscle (Blumer et al., 2017). Palisade endings were described as sensory structures based on their morphology (Ruskell, 1978; Alvarado-Mallart and Pinçon-Raymond, 1979). Nonetheless, their function is under debate as connectional and molecular characteristics suggest a motor role, that is, palisade endings are cholinergic, are traced from the oculomotor nuclei, contain key proteins of the exocytotic machinery but lack, however, postsynaptic nicotinic acetylcholine receptors and have little, if any, extracellular acetylcholinesterase (Blumer et al., 2009, 2016, 2020; Zimmermann et al., 2013).

Given that oculomotor organization is more complex than initially devised, we aimed at describing the function of electrophysiologically-identified MIF motoneurons innervating the medial rectus muscle and its relative contribution to the different types of eye movements.

Materials and Methods

Ethics statement

All procedures were performed in accordance with the guidelines of the European Union (2010/63/EU) and the Spanish legislation (R.D. 53/2013, BOE 34/11370-421) for the use and care of laboratory animals and approved by the ethics committee (protocol #13/04/2018/047). All efforts were made to reduce the number of animals used.

Animals and surgical procedures

Experiments were performed on adult female cats weighing 2.0–2.5 kg obtained from authorized suppliers (Universidad de Córdoba, Spain). A total of 8 animals was used for the present study. Five of them were prepared for extracellular single-unit recordings of medial rectus motoneurons in the oculomotor nucleus (Fig. 1*A*), and the other three for the morphologic study. None of these three cats used for morphology derived from electrophysiological experiments.

Animals were prepared for chronic recordings as previously described (de la Cruz et al., 1989; Hernández et al., 2017). Briefly, atropine sulfate (0.5 mg/kg, i.m.) was injected to reduce vagal reflexes and ketamine hydrochloride (20 mg/kg, i.m.) mixed with xylazine (0.5 mg/kg, i.m.) to induce anesthesia. Thereafter, animals were placed in a stereotaxic frame. Surgery was performed under sterile conditions to implant stimulating electrodes, scleral coils, and the recording chamber (Fig. 1*A*). For the antidromic identification of the oculomotor nucleus, silver bipolar electrodes were implanted in the third nerve bilaterally (Fig. 1*A*, St. 1). In addition, a pair of hook electrodes, made of three-strand stainless steel Teflon insulated wire was inserted at the myotendinous junction of both medial rectus muscles to activate (Eladly et al., 2020) the axons of MIF motoneurons (Fig. 1*A*, St. 2). Hook electrodes were located ~10 mm apart from the muscle's belly where the band of en plaque contacts of SIF motoneurons is located. It has been shown that, because of volume conduction attenuation, the current decays in muscle to 10% over a 10 mm distance (Enoka et al., 2020). The criterion for stimulating MIF axons was 1–1.1× the threshold to produce a maximal field potential from the tendon electrode using currents always $<100\ \mu A$. Coils, made up of two turns of Teflon-isolated stainless-steel wire, were implanted in the sclera of both eyes for the recording of eye movements (Fig. 1*A*). A square window (6 × 6 mm) was drilled in the parietal bone to allow the lateral access to the midbrain oculomotor nucleus. A restraining system was also constructed to immobilize the head during the recordings. Postoperative care was provided daily, as needed, to ensure the healthy state of the animal.

Chronic extracellular recordings

After 10 d of postoperative recovery, recording sessions started. The animal was comfortably seated in a fabric bag, bandaged, and placed in a Perspex box, which was located inside the magnetic field for eye movement recordings (Fuchs and Robinson, 1966). Extracellular recordings were conducted with glass micropipettes, filled with 2 M sodium chloride, attached to a three-axis micromanipulator to advance through the intact brain to reach the medial rectus subdivision of the oculomotor nucleus. The oculomotor nucleus was located by its antidromic field potential after the electrical stimulation to the ipsilateral IIIrd nerve (50-μs pulses of <0.1 mA). The medial rectus subdivision was located stereotaxically and medial rectus motoneurons were identified, as previously described (Hernández et al., 2017), by their increase in firing frequency selectively during nasally-directed horizontal eye movements. In addition, the collision test of the orthodromic and antidromic spike was systematically used to assure that the activated unit was indeed the recorded one.

Both MIF and SIF medial rectus motoneurons were antidromically activated from the electrode placed at the third nerve (collision tests in Fig. 1*B*,*C*, IIIn). This procedure indicated that the axons of both types of units coursed through the oculomotor nerve. MIF motoneurons were distinguished from SIF motoneurons because only the former were antidromically activated from the electrode located at the myotendinous junction (collision tests in Fig. 1*B*,*C*, MTJ). Once identified, the extracellular action potentials of the motoneuron were recorded along with eye movements under alert conditions. For some cells, it was also possible to record their firing during vestibularly-induced eye movements in the horizontal plane by means of a servo-controlled motor attached to the turntable oscillating at a frequency of 0.125 Hz and ±20° peak-to-peak amplitude.

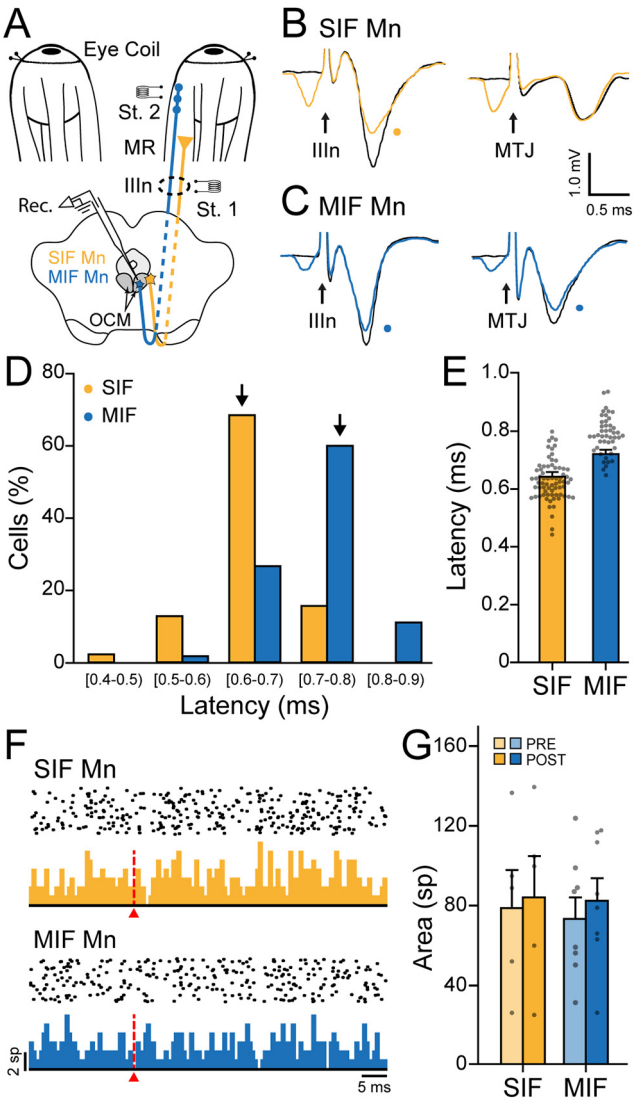

Figure 1. Experimental design and electrophysiological identification of SIF and MIF motoneurons. ***A***, Diagram illustrating the methodological approach for recordings. Motoneurons innervating the medial rectus muscle (MR) are located in the midbrain oculomotor nucleus (OCM), where recordings (Rec.) were performed under alert conditions. Both, MIF and SIF motoneurons were antidromically activated from the stimulating electrode located at the III nerve (IIIn, St. 1). Only MIF motoneurons were, in addition, antidromically activated from the stimulating electrode placed at the myotendinous junction of the MR muscle (St. 2). Eye coils were implanted in the sclera of both eyes for the recording of eye movements. ***B***, ***C***, Collision tests were used to distinguish between SIF and MIF motoneurons. In ***B***, the orthodromic spike of a SIF motoneuron collided with the antidromic spike (when the orthodromic spike was at a short latency) after electrical stimulation to the IIIn (collision shown by an orange dot). However, this cell showed no collision after applying electrical stimulation to the electrode placed at the myotendinous junction (MTJ). On the other hand, MIF motoneurons (***C***) showed collision from both stimulating electrodes (IIIn and MTJ; blue dots). The arrows point to the onset of the stimulus artifact. ***D***, Distribution of antidromic latencies from the IIIn stimulus of SIF (orange) and MIF (blue) motoneurons grouped at time intervals of 0.1 ms. Arrows point to the mean of each motoneuronal population. In the abscissa axis, brackets include the first number in the interval and parentheses exclude the last number in the interval. ***E***, Bar chart showing the mean ± SEM of the antidromic latencies of SIF and MIF motoneurons following IIIn stimulation. SIF motoneurons showed a significantly lower mean antidromic latency (asterisk) as compared with MIF motoneurons (*t* test, $p < 0.001$, $n = 70$ and $n = 45$ SIF and MIF motoneurons, respectively). ***F***, PSTHs generated for a SIF and a MIF motoneuron after electrical stimulation at the myotendinous junction of the medial rectus muscle illustrating 20 ms before and 50 ms after stimulation (in spikes, sp). The stimulus artifact bin has been deleted and is represented as a red arrowhead and dashed vertical line. Bin width for PSTHs is 0.5 ms. The raster mode is shown for each motoneuron above its respective PSTH. ***G***, Quantification of the PSTH responses for SIF and MIF motoneurons measured as the area, in spikes, obtained as the number of counts (in spikes) during the 20-ms period before (PRE, striped bars) and for the 20-ms period after (POST, solid bars) the stimulus. Comparison of areas obtained 20 ms before versus 20 ms after the stimulation revealed no significant differences for both SIF (Wilcoxon signed-rank test, $p = 0.125$, $n = 5$) and MIF (Wilcoxon signed-rank test, $p = 0.250$, $n = 8$) motoneurons. Data are mean and SEM.

Peristimulus time histograms (PSTHs) were conducted following the repetitive electrical stimulation to the electrode placed at the myotendinous junction simultaneously with the recording of an identified MIF or SIF motoneuron, to check whether the activation of palisade endings could change the probability of discharge of the recorded motoneuron. Parameters to generate the PSTHs were the same as we have used previously (Davis-López de Carrizosa et al., 2009).

Data storage and analysis

Horizontal eye position (EP) and associated neuronal activity were digitally stored for off-line analysis (Power 1401, Cambridge Electronic Design). Computer programs written in MATLAB 7.5 were used for selecting the data of instantaneous firing frequency along with the corresponding EP and eye velocity (EV). The correlations between firing rate (FR) and EP and EV were conducted according to the equation $FR = F_0 + k \cdot EP + r \cdot EV$, where k and r are the neuronal sensitivities to EP (k, in spikes/s/°) and velocity (r, in spikes/s/°/s), and F_0 is the FR at straight ahead gaze, that is, when EP = 0° (Robinson, 1970; de la Cruz et al., 1989; Davis-López de Carrizosa et al., 2011). During spontaneous eye fixations, EV = 0, and therefore this equation can be expressed as $FR = F_0 + k \cdot EP$. Accordingly, the correlation between FR and EP was fitted by a linear regression line where the slope of the line represents the neuronal EP sensitivity (k). The intercept of the line with the abscissa axis represents the estimated EP threshold for recruitment (Robinson, 1970; Delgado-Garcia et al., 1986). To obtain the neuronal eye sensitivity during spontaneous rapid eye movements, or saccades, we correlated FR, after the subtraction of the previously calculated EP component ($k \cdot EP - F_0$), with EV during saccades, according to the equation $FR - k \cdot EP - F_0 = r \cdot EV$, by means of linear regression analysis.

During vestibularly-induced eye movements, neuronal EP and EV were obtained by multiple linear regression using the equation $FR = F_0 + k \cdot EP + r \cdot EV$, selecting between cursors only the slow phases of the nystagmus. We named k_s and r_s to neuronal EP and EV sensitivities, respectively, obtained during spontaneous eye movements, and k_v and r_v to neuronal EP and EV sensitivities calculated during vestibular eye movements. Correlations between FR and EP and EV were made with the eye ipsilateral to the recorded nucleus.

Morphologic identification of MIF motoneurons

Retrograde labeling of rhodamine B isothiocyanate (Sigma-Aldrich) was used to identify MIF motoneurons. Animals were anesthetized as described above and placed in a stereotaxic frame. The medial rectus muscle was isolated under a dissecting microscope and with the help of a muscle hook, 1 µl of 20% rhodamine dissolved in 2% dimethylsulfoxide was injected at the myotendinous junction of the medial rectus muscle to selectively label only MIF motoneurons, according to previous reports (Büttner-Ennever et al., 2001; Eberhorn et al., 2006; Bohlen et al., 2017b; Hernández et al., 2019).

Two weeks after rhodamine injection, animals were transcardially perfused under deep anesthesia (sodium pentobarbital, 100 mg/kg, i.p.) with 500 ml of saline followed by fixative (4% paraformaldehyde prepared in 0.1 M phosphate buffer, pH 7.4). The brainstem was removed and cut on a vibratome in coronal sections of 50-µm thickness. Medial rectus muscles were dissected to reveal the extent of rhodamine injection.

Immunofluorescence for confocal microscopy

For the identification of motoneurons, choline acetyltransferase (ChAT), the biosynthetic enzyme for acetylcholine, was used.

Double immunofluorescence was used to combine ChAT with synaptic markers, either synaptophysin (a general marker of synaptic boutons) or vesicular GABA and glycine amino acid transporter (VGAT), to selectively label inhibitory boutons. MIF medial rectus motoneurons were, in addition, retrogradely labeled with rhodamine. Therefore, we focused within the medial rectus subdivision and distinguished MIF medial rectus motoneurons as those that were for rhodamine-positive and ChAT-immunoreactive (IR), whereas SIF medial rectus motoneurons were those ChAT-IR motoneurons that lacked the retrograde rhodamine labeling.

For immunofluorescence, we used as primary antibodies: (1) goat polyclonal antibody against ChAT (1:500; Millipore); (2) mouse monoclonal antibody against synaptophysin (1:1000; Millipore); and (3) rabbit polyclonal antibody against VGAT (1:500; Millipore). Secondary antibodies were: (1) donkey anti-goat IgG coupled to FITC (to detect ChAT); (2) donkey anti-mouse IgG coupled to Cy5 (to reveal synaptophysin); (3) and donkey anti-rabbit IgG coupled to Cy5 (for VGAT visualization). All secondary antibodies were used at a dilution of 1:50 (Jackson ImmunoResearch). Images were captured with a confocal microscope (Zeiss LSM 7 DUO) using different filters with the Zeiss microscope program ZEN.

Morphologic analysis

The following analyses were performed using the captured confocal images: (1) the topographic distribution of MIF medial rectus motoneurons within the oculomotor nucleus; (2) the somatic size of SIF and MIF motoneurons; and (3) the synaptic coverage around cell bodies with either synaptophysin or VGAT, in both SIF and MIF motoneurons. The distribution of MIF medial rectus motoneurons within the oculomotor nucleus was conducted using 4×4 tile confocal images at $10\times$ magnification to visualize the entire nucleus. The topographical analysis was performed using the Adobe Illustrator program (Adobe Systems Incorporated). For the measurement of the somatic size of both motoneuronal types, three parameters were calculated: (1) the average of the large and small diameter; (2) the cell body area; and (3) the somatic perimeter. For these measurements, stacks of confocal planes of 1-μm virtual thickness captured at $63\times$ magnification were used, selecting the plane at which the cell nucleus showed its maximum diameter. The program ImageJ (NIH) was used to calculate cell size parameters. Synaptic coverage around SIF and MIF motoneurons was measured as the percentage of the somatic perimeter that appeared surrounded by immunoreactive boutons, either synaptophysin-IR or VGAT-IR.

Statistics

To compare morphologic and physiological measurements between SIF and MIF motoneurons the Student's *t* test, the two-way ANOVA, the Wilcoxon signed-rank test or the Mann–Whitney rank-sum test were used at a level of significance of $p < 0.05$ (SigmaPlot 11 program; Systat Software). All regression analyses were significant ($p < 0.05$). The effect size was measured as Cohen's *d* (*d*) and determined with online calculators (https://www.psychometrica.de/effect_size.html). Data are shown as mean ± SEM.

Results

Electrophysiological identification of SIF and MIF medial rectus motoneurons

When a unit was isolated within the limits of the medial rectus subdivision of the oculomotor nucleus, we systematically proceeded to characterize the unit as either MIF or SIF motoneuron by the antidromic activation and collision test performed from the electrodes placed at the IIIrd nerve (Fig. 1*A*, St.1) and in the myotendinous junction of the medial rectus muscle (Fig. 1*A*, St. 2). The unit was considered to be a SIF motoneuron if it was antidromically activated and collided after the electrical stimulation to the IIIrd nerve, but activation and collision failed from the electrode placed at the myotendinous junction (Fig. 1*B*, see collision from the IIIrd nerve at the left of the panel, and failure of collision after electrical stimulation to the myotendinous junction, at the right of the panel). On the other hand, MIF motoneurons were identified because they were antidromically activated and collided from both electrodes, that is, from the IIIrd nerve and from the myotendinous junction (Fig. 1*C*).

To evaluate whether there was a difference in the antidromic latencies from the nerve between MIF and SIF motoneurons, the time interval between the onset of the stimulus artifact and the negative peak of the spike was measured. Figure 1*D* illustrates the distribution of antidromic latencies for MIF and SIF medial rectus motoneurons. As can be observed, the distribution of latencies for MIF motoneurons was displaced toward the right, thus toward higher latency values. The arrows in Figure 1*D* point to the mean antidromic latency for both motoneuronal types, illustrating a higher latency for the MIF population of motoneurons. When MIF and SIF motoneurons were pooled in two groups, the statistical comparison of antidromic latencies between both populations revealed that MIF motoneurons showed a significantly higher antidromic activation latency when compared with SIF motoneurons (0.723 ± 0.009 and 0.644 ± 0.007 ms, respectively; *t* test, $t_{(113)} = 6.750$, $p < 0.001$, $d = 1.29$; $n = 45$ MIF and $n = 70$ SIF motoneurons; Fig. 1*E*).

Peristimulus time intervals (PSTHs) were performed after repetitive stimulation (>150 pulses, 1 Hz) to the electrode placed at the myotendinous junction while recording the extracellular potentials of an identified MIF or SIF motoneuron to determine whether palisade ending stimulation could exert any synaptic influence on the motoneuron discharge probability. We constructed binned histograms (bin width 0.5 ms) from 20 ms before to 50 ms after the stimulation, with the stimulus artifact pooled at time 0 bin, but excluded from computations (Davis-López de Carrizosa et al., 2009). The stimulus intensity applied was the minimum to obtain the maximum antidromic field potential from the muscle-tendon electrode. An example of the PSTH for a SIF and for a MIF motoneuron is illustrated in Figure 1*F*. In both motoneuronal types, it can be appreciated that the discharge before and after the stimulation (indicated by the red arrowhead and vertical dashed line) shows similar rates. To quantify PSTHs, we obtained the number of counts (in spikes) during the initial 20 ms (before stimulation) and compared this value with the 20-ms period after stimulation. The results indicated absence of significant differences in the PSTHs (Fig. 1*G*) for both types of motoneuron (Wilcoxon signed-rank test, $Z = 1.260$, $p = 0.250$, $n = 8$ for MIF motoneurons and $Z = 1.753$, $p = 0.125$, $n = 5$ for SIF motoneurons).

Firing pattern of MIF and SIF medial rectus motoneurons during spontaneous, convergent, and vestibularly-induced eye movements

Medial rectus motoneurons showed a tonic-phasic discharge pattern in correlation with eye movements, as previously described (de la Cruz et al., 1989). During fixations, medial rectus motoneurons fired tonically, with higher rates for nasal-directed EPs, that is, movements contralateral to the recording side (on direction). During rapid eye movements or saccades, these motoneurons discharged a high-frequency burst of spikes for on-directed saccades, and a pause or an abrupt firing decay for off-directed saccades. As shown in Figure 2*A*,*B*, the discharge of MIF and SIF motoneurons during spontaneous eye movements revealed that both motoneuronal types discharged in a tonic-phasic way. However, MIF motoneurons displayed overall lower FRs compared with SIF motoneurons (Fig. 2*A*,*B*).

The behavior of MIF and SIF medial rectus motoneurons during spontaneous convergent eye movements was also

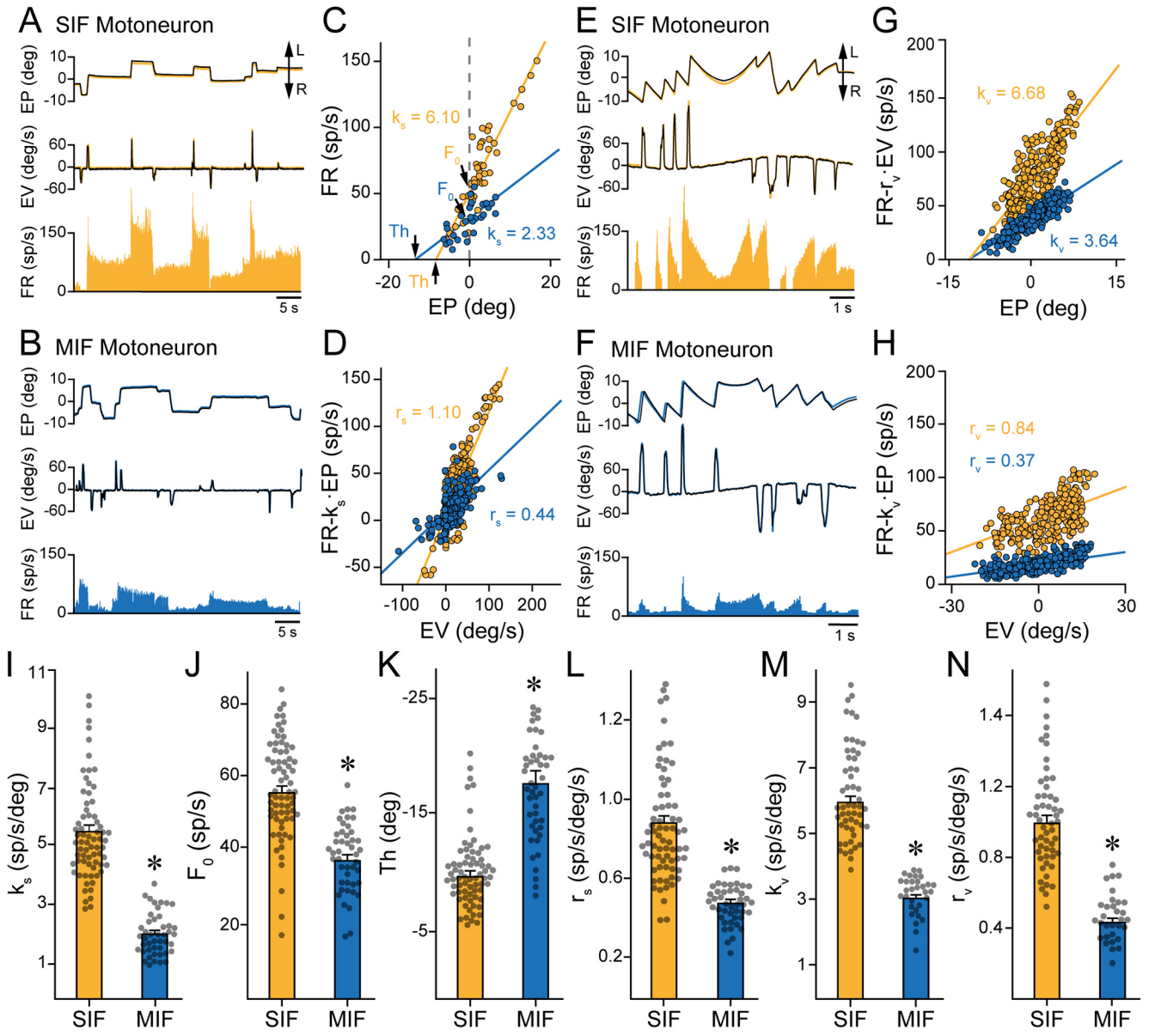

Figure 2. Discharge of SIF and MIF medial rectus motoneurons during spontaneous and vestibular eye movements. ***A***, ***B***, Examples of the discharge of a SIF (***A***) and a MIF (***B***) motoneuron during spontaneous eye movements. From top to bottom, traces illustrate: EP (in degrees), EV (in °/s), and FR (in spikes/s). EP and EV are shown as overlapping traces for both eyes, the color trace corresponds to the eye homolateral to the recorded motoneuron (right side). Leftwards and rightwards eye movements are indicated by the double arrow as L and R, respectively. ***C***, Regression lines between FR and EP for the two motoneurons illustrated in ***A***, ***B*** during eye fixations. The FR at straight ahead gaze (F_0) and the threshold (Th) are indicated, as well as k_s (EP sensitivity, the slope of the regression line) with its respective value for each motoneuron. ***D***, Regression lines between FR (previous subtraction of the EP component) and EV for the motoneurons shown in ***A***, ***B*** during saccades. The slope of these regression lines corresponds to r_s (EV sensitivity), whose value is indicated for each motoneuron. ***E***, ***F***, Discharge pattern of a SIF (***E***) and a MIF (***F***) motoneuron during vestibularly-induced eye movements. Traces are as indicated in ***A***, ***B***. ***G***, ***H***, Partial regression plots of FR minus the velocity component versus EP (***G***), and FR minus the position component versus EV (***H***) obtained during vestibular eye movements. EP (k_v) and EV (r_v) sensitivities of these two motoneurons are indicated. ***I–L***, Bar charts comparing k_s, F_0, Th, and r_s during spontaneous eye movements between SIF ($n = 70$) and MIF ($n = 45$) motoneurons. ***M***, ***N***, Bar charts comparing k_v and r_v between SIF ($n = 54$) and MIF ($n = 31$) motoneurons during vestibular eye movements. For ***I–N***, data are mean ± SEM, and comparisons were performed with *t tests*, in all cases $p < 0.001$ (asterisks).

evaluated. The great majority of MIF and SIF motoneurons increased their firing during convergence, as expected (for SIF motoneurons: 154 epochs of convergence, in 45 cells, with 83.8% of appropriate responses; for MIF: 87 epochs of convergence, in 27 cells, with 86.2% of appropriate response). It is important to emphasize that in any case neither MIF nor SIF medial rectus motoneurons displayed an inappropriate response (i.e., a decrease in FR) for convergent eye movements, in contrast with the inappropriate firing we reported previously for a small percentage of MIF and SIF abducens motoneurons during divergences (Hernández et al., 2019).

During vestibularly-induced eye movements, medial rectus motoneurons discharged in proportion to EP and EV, increasing their FR for eye movements in the nasal direction, during both the slow and the fast phases of the nystagmus, and decreasing their FR in the opposite direction. As occurred during spontaneous eye movements, MIF motoneurons discharged at lower firing frequencies as compared with SIF motoneurons during vestibularly-induced eye movements (Fig. 2*E*,*F*).

Quantitative comparison of eye-related parameters between MIF and SIF medial rectus motoneurons during spontaneous and vestibular eye movements

For spontaneous eye movements, we calculated neuronal EP sensitivity (k_s) as the slope of the rate-position plot during eye fixations, when the velocity component was zero. The regression lines between FR and EP (Fig. 2*C*) for the motoneurons shown in Figure 2*A*,*B* illustrated the method of analysis to calculate k_s (the slope of the regression line), F_0 (the FR at straight ahead gaze, when EP is zero), and the recruitment threshold (Th; the EP at which the motoneuron is recruited into activity). To calculate neuronal eye EP and EV during saccades, FR (after subtracting the EP component) was plotted versus EV (Fig. 2*D*). The slope of the regression line thus obtained corresponded to neuronal eye velocity sensitivity (r_s). Note in Figure 2*D* that for the MIF motoneuron illustrated in Figure 2*B*, its r_s value was lower than that of the SIF motoneuron shown in Figure 2*A*.

Therefore, we proceeded to compare these four parameters, obtained during spontaneous eye movements (k_s, F_0, Th, and r_s), between the whole population of SIF ($n = 70$) and MIF ($n = 45$) motoneurons. For k_s, SIF motoneurons showed a mean of 5.59 ± 0.19 and MIF motoneurons 2.17 ± 0.10 spikes/s/°. The statistical analysis demonstrated that MIF motoneurons showed a significantly lower mean k_s as compared with SIF motoneurons (*t* test, $t_{(113)} = -13.125$, $p < 0.001$, $d = -2.508$; Fig. 2*I*). F_0 was also significantly lower for MIF motoneurons (35.56 ± 1.25 spikes/s) than for SIF motoneurons (53.02 ± 1.48 spikes/s), as can be appreciated in Figure 2*J* (*t* test, $t_{(113)} = -8.294$, $p < 0.001$, $d = -1.585$). MIF motoneurons were recruited at more eccentric EPs in the off-direction than SIF motoneurons, thereby presenting lower thresholds (-18.12 ± 1.04° vs -10.30 ± 0.45°, respectively; Fig. 2*K*). The difference in thresholds between both motoneuronal types was also significant (*t* test, $t_{(113)} = -7.794$, $p < 0.001$, $d = -1.489$). During saccades, EV sensitivity (r_s) reached lower values for MIF than for SIF motoneurons (0.49 ± 0.02 vs 0.89 ± 0.03 spikes/s/°/s, respectively) yielding a significant difference (*t* test, $t_{(113)} = -9.289$, $p < 0.001$, $d = -1.775$; Fig. 2*L*).

There were also differences between the firing of MIF and SIF motoneurons during on-directed saccades. Thus, the latency between the saccade onset and the peak FR occurred ~9 ms later in MIF motoneurons than in SIF motoneurons (64.2 ± 1.35 vs 55.3 ± 1.28 ms, respectively), a difference that was significant (*t* test; $t_{(413)} = 4.797$, $p < 0.001$, $d = 0.451$). Peak FR preceded peak saccadic velocity for both motoneuron types. However, the peak firing of MIF motoneurons was closer to peak saccadic velocity (6.5 ms; paired *t* test, $t_{(206)} = 10.251$, $p < 0.001$, $d = 0.349$), whereas SIF motoneurons fired maximally with a longer latency preceding peak EV (13.4 ms; paired *t* test, $t_{(207)} = 23.810$, $p < 0.001$, $d = 0.763$). These findings suggest that MIF motoneurons contributed mainly during the last part of the saccade, which requires a fine adjustment to set the eye still on visual target while relaxing the viscoelastic forces implied in the saccade. On the other hand, SIF motoneurons were more influential for starting the saccade and reaching its peak velocity, when more force is needed to overcome the viscoelastic properties of the oculomotor plant. Similar differences were also found between MIF and SIF motoneurons of the abducens nucleus (Hernández et al., 2019).

During vestibularly-induced eye movements, neuronal EP and EV sensitivities (k_v and r_v, respectively) were calculated by multiple regression analysis and compared between MIF ($n = 31$) and SIF ($n = 54$) motoneurons. Partial regression plots of FR versus EP (Fig. 2*G*) or EV (Fig. 2*H*) for the SIF and MIF motoneurons illustrated in Figure 2*E*,*F*, respectively, clearly showed that both sensitivities (k_v and r_v) were higher for the SIF than for the MIF motoneurons. As a pool, MIF motoneurons showed lower k_v values (3.07 ± 0.11 spikes/s/°) as compared with SIF (5.99 ± 0.19 spikes/s/°) motoneurons (Fig. 2*M*), reaching statistical significance (*t* test, $t_{(83)} = -11.100$, $p < 0.001$, $d = -2.501$). The same happened with r_v, which was significantly lower for MIF motoneurons (0.43 ± 0.02 spikes/s/°/s) with respect to SIF motoneurons (0.99 ± 0.05 spikes/s/°/s), as can be appreciated in Figure 2*N* (*t* test, $t_{(83)} = -8.956$, $p < 0.001$, $d = 2.018$).

Recruitment order and correlations between parameters in MIF and SIF medial rectus motoneurons

According to the analyses described above, MIF medial rectus motoneurons discharged at lower FRs and with lower sensitivities, and were recruited first, as compared with SIF medial rectus motoneurons. These differences can be clearly appreciated in the plots of Figure 3*A*,*B*, in which the entire samples of 70 SIF and 45 MIF motoneurons were represented. Thus, MIF motoneurons showed lower slopes in their rate-position (Fig. 3*A*) and rate-velocity (Fig. 3*B*) plots, reaching for a given EP or EV lower values of firing frequency, as compared with the SIF motoneuron population. In addition, MIF motoneurons started their discharge at more negative EPs, i.e., with the eye located more laterally in the orbit (the off direction for medial rectus motoneurons), indicating that they had lower recruitment thresholds (Fig. 3*A*). Since MIF motoneurons had longer antidromic latencies and smaller cell size (see below), the present data are in congruence with the size principle (Henneman et al., 1965), so that smaller motoneurons are recruited first and contribute generating less force than larger motoneurons.

Correlations between these parameters (k_s, Th, r_s) have been described previously for extraocular motoneurons considered as a homogeneous pool (Delgado-Garcia et al., 1986; Fuchs et al., 1988; Pastor and González-Forero, 2003; Davis-López de Carrizosa et al., 2011; Hoh, 2021). We aimed at investigating whether similar relationships could be present in MIF and SIF medial rectus motoneurons treated as separate populations. Results are shown in Figure 3*C*–*E*. First, when correlating k_s with threshold, a significant exponential fit was found for both motoneuronal types (Fig. 3*C*), so that the higher the threshold (less negative EPs), the higher the EP sensitivity (k_s), for both MIF (blue dots and line, $r = 0.719$, $p < 0.001$) and SIF motoneurons (orange dots and line, $r = 0.801$, $p < 0.001$). It was also observed that lower k_s and thresholds were present in MIF motoneurons as compared with SIF motoneurons. Figure 3*C*, black line, represents the exponential fit of the whole population of MIF + SIF motoneurons ($r = 0.798$, $p < 0.001$). Second, the correlation between k_s and r_s also fitted to an exponential equation (Fig. 3*D*), for both MIF ($r = 0.542$, $p < 0.001$) and SIF ($r = 0.794$, $p < 0.001$) motoneurons, meaning that motoneurons with higher k_s values also presented, in general, higher r_s values. Figure 3*D*, black line, represents the correlation k_s versus r_s for the entire population of MIF and SIF motoneurons, which also fitted to an exponential equation ($r = 0.834$, $p < 0.001$). Third, the correlation between r_s and threshold was significant for SIF motoneurons ($r = 0.652$, $p < 0.001$; Fig. 3*E*, orange dots and line), but not for MIF motoneurons (Fig. 3*E*, blue dots). However, when both motoneuronal types were grouped as a single population, an

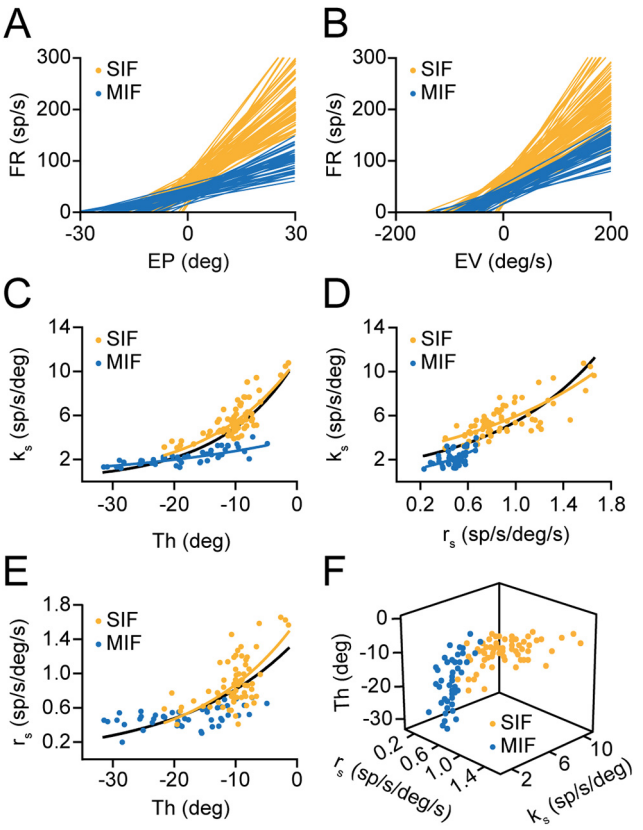

Figure 3. Recruitment order and correlations between SIF and MIF medial rectus motoneurons during spontaneous eye movements. ***A***, Linear regression lines obtained for SIF and MIF motoneurons between FR and EP. ***B***, Same as ***A***, but for the relationship between FR and EV. ***C***, Correlations between k_s and Th for either SIF, MIF, or the entire population (MIF + SIF) of motoneurons (black line) according to the exponential fit equations: $y = 11.170 \cdot e^{0.071x}$ ($r = 0.801$, $p < 0.001$), $y = 3.840 \cdot e^{0.034x}$ ($r = 0.719$, $p < 0.001$), and $y = 11.106 \cdot e^{0.082x}$ ($r = 0.798$, $p < 0.001$) for SIF, MIF, and all motoneurons, respectively. ***D***, Relationships between k_s and r_s for SIF, MIF, and the whole pool of motoneurons (MIF + SIF; black line) fitted by the following exponential equations: $y = 2.773 \cdot e^{0.765x}$ ($r = 0.794$, $p < 0.001$), $y = 0.857 \cdot e^{1.879x}$ ($r = 0.542$, $p < 0.001$), and $y = 1.821 \cdot e^{1.096x}$ ($r = 0.834$, $p < 0.001$), for SIF, MIF, and all motoneurons, respectively. ***E***, Correlation between r_s and Th for SIF motoneurons fitted to the exponential equation $y = 1.621 \cdot e^{0.061x}$ ($r = 0.652$, $p < 0.001$). The group of MIF motoneurons did not show a significant correlation between r_s and Th, but the entire pool of motoneurons (MIF + SIF; black line) did fit by the exponential equation $y = 1.393 \cdot e^{0.054x}$ ($r = 0.647$, $p < 0.001$). ***F***, Scatterplot of k_s, Th and r_s for SIF and MIF motoneurons. For all plots (***A–F***), $n = 70$ SIF and $n = 45$ MIF motoneurons.

exponential equation resulted from the relationship between r_s and threshold (black line, $r = 0.647$, $p < 0.001$).

When k_s, Th and r_s values were represented in a 3D plot (Fig. 3*F*) for MIF and SIF motoneurons, the two motoneuronal types distributed, in general, as distinct populations. Thus, it can be clearly appreciated that MIF motoneurons (blue dots) grouped toward lower Th, r_s and k_s values as compared with SIF motoneurons (orange dots).

Distribution of MIF medial rectus motoneurons within the oculomotor nucleus

The retrograde tracer rhodamine, injected at the myotendinous junction of the medial rectus muscle (Fig. 4*A*, top) was used to anatomically identify MIF medial rectus motoneurons in the oculomotor nucleus. We obtained similar results for the three animals processed for this purpose. MIF motoneurons appeared located within the medial rectus subdivision of the oculomotor complex, that is, in the rostral two thirds of this nucleus, both at the dorsal and ventrolateral groups, with more MIF motoneurons found in the dorsal group (Fig. 4*A*), the main subgroup of the medial rectus motoneuron pool in cats (Akagi, 1978; Miyazaki, 1985; de la Cruz et al., 1994; Büttner-Ennever, 2006). However, as illustrated in Figure 4*B–D*, some MIF motoneurons appeared in the ventrolateral group, some of them interspersed among the bundles of the medial longitudinal fascicle. A previous study in cats has described MIF medial rectus motoneurons mainly in the ventrolateral subgroup, in accordance with our work, although we also found them in the dorsal pool (Bohlen et al., 2017b).

To determine the percentage of MIF motoneurons with respect to the total population of medial rectus motoneurons, rhodamine-positive motoneurons (MIF) were counted and compared with the total number of ChAT-IR motoneurons (SIF+MIF) located at the medial rectus motoneuron subdivision of the oculomotor nucleus (Akagi, 1978; Miyazaki, 1985; de la Cruz et al., 1994; Büttner-Ennever, 2006). The results indicated that the number of MIF motoneurons in relation to the population of medial rectus motoneurons was, on average, 23.77%. The proportion found of MIF motoneurons is in agreement with previous reports in monkeys (Büttner-Ennever et al., 2001), rats (Eberhorn et al., 2006), and in the cat abducens nucleus (Hernández et al., 2019).

Differences between MIF and SIF medial rectus motoneurons in cell size and synaptic coverage

To compare the somatic cell size between MIF and SIF motoneurons, three parameters were measured (average diameter, area, and perimeter) in ChAT-IR motoneurons. We obtained significant differences between both motoneuronal groups, with MIF motoneurons showing significantly lower average diameter (28.87 ± 0.35 µm; *t* test, $t_{(528)} = -11.155$, $p < 0.001$, $d = -1.138$), area [651.21 ± 14.94 µm^2 (Fig. 4*E*); *t* test, $t_{(528)} = -8.762$, $p < 0.001$, $d = -0.894$ (Fig. 4*F*)], and perimeter (95.82 ± 1.06 µm; *t* test, $t_{(528)} = -9.917$, $p < 0.001$, $d = -1.012$; Fig. 4*G*) in comparison with SIF motoneurons (34.05 ± 0.24 µm, 866.75 ± 12.92 µm^2, 110.50 ± 0.76 µm, for average diameter, area, and perimeter, respectively). The number of motoneurons analyzed was $n = 126$ MIF and $n = 404$ SIF motoneurons for the three measurements.

The overall lower FR of MIF motoneurons led us to study the density of synaptic terminals that MIF motoneurons receive on their cell body and to compare this value with that of SIF motoneurons. We did this study using immunocytochemistry against synaptophysin, as a general marker for both excitatory and inhibitory boutons, as well as against VGAT, a selective marker of inhibitory boutons. By confocal microscopy, the percentage of the somatic perimeter that was contacted by either synaptophysin-IR or VGAT-IR (i.e., linear density, in %) was calculated.

Regarding synaptophysin, it was observed that MIF motoneurons were covered by less synaptic boutons as compared with SIF motoneurons. This can be appreciated in the SIF and MIF motoneurons illustrated in Figure 5*B*,*C*, respectively, whose location in the oculomotor nucleus is indicated by white arrows in Figure 5*A*. When all measured motoneurons were grouped, the statistical analysis of synaptophysin coverage (an index of synaptic linear density) yielded a significant difference, with MIF ($n = 65$) motoneurons showing a significantly lower synaptic coverage than SIF ($n = 206$) motoneurons ($31.64 \pm 0.96\%$ and $51.84 \pm 0.60\%$, respectively; *t* test, $t_{(269)} = -16.933$, $p < 0.001$, $d = -2.409$; Fig. 5*D*).

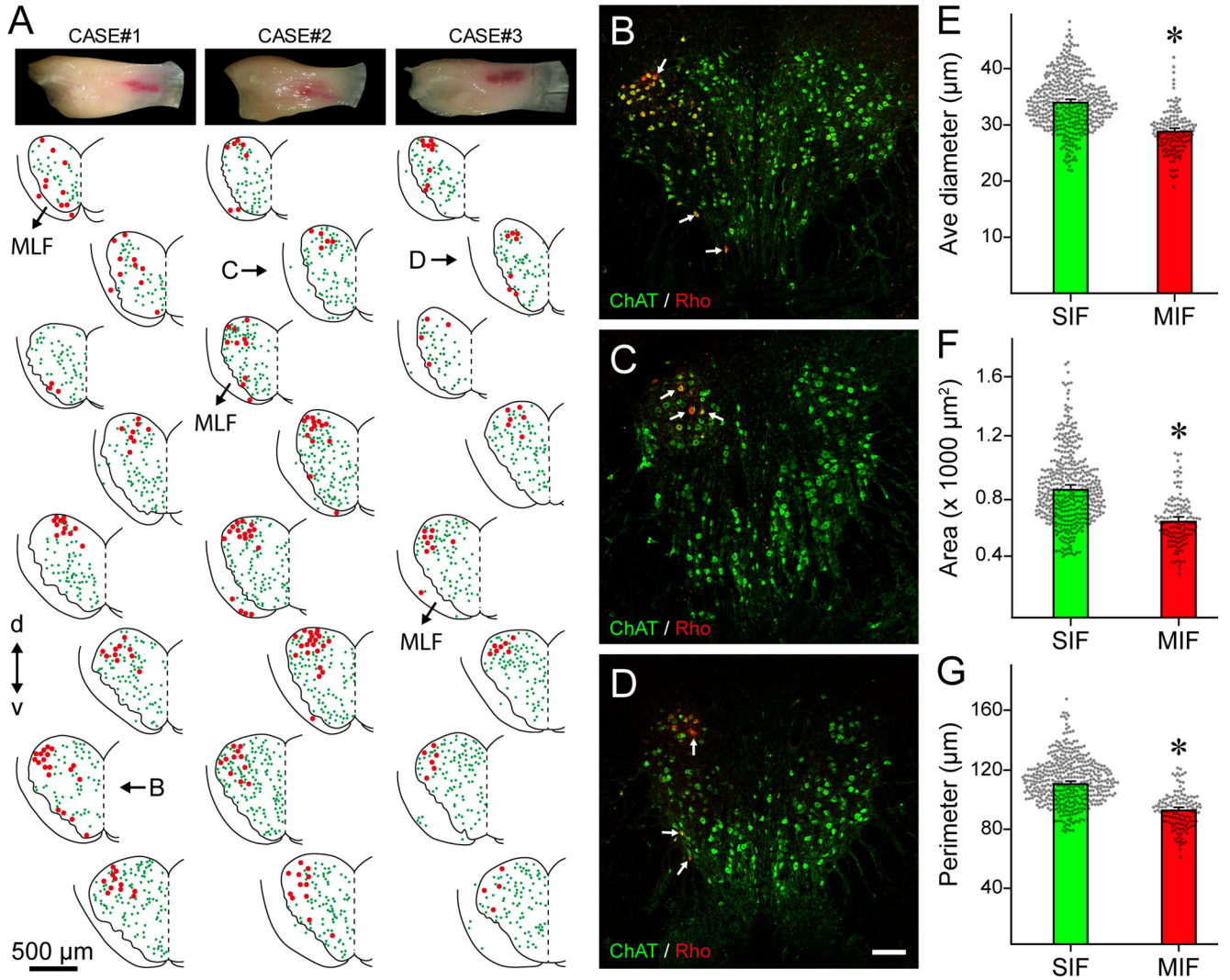

Figure 4. Topographic distribution of MIF medial rectus motoneurons within the oculomotor nucleus and cell size measurements. ***A***, For the location of MIF medial rectus motoneurons, rhodamine (in red) was injected as a retrograde tracer into the myotendinous zone of the medial rectus muscle. Rhodamine was combined with ChAT immunostaining (in green), as a marker of both MIF and SIF motoneurons. The drawings illustrate the distribution pattern of both motoneuronal types in histologic sections throughout the oculomotor nucleus, from rostral (top) to caudal (bottom), in three different animals. Rhodamine injection in the medial rectus muscle is shown at the top for each animal. The vertical dashed line in each drawing corresponds to midline; MLF stands for medial longitudinal fascicle. Dorsal and ventral are indicated as d and v, respectively. ***B–D***, Confocal images of the oculomotor nucleus of each animal. Each image corresponds to the drawing indicated in panel ***A*** as ***B***, ***C***, or ***D***, respectively. Small white arrows in ***B–D*** point to some MIF medial rectus motoneurons, which were identified as doubly-labeled, i.e., rhodamine-positive (Rho) and ChAT-IR. ***E–G***, Bar charts illustrating the mean ± SEM of the somatic average diameter (***E***), area (***F***), and perimeter (***G***) of 404 SIF and 126 MIF motoneurons. In the three cell size measurements, MIF motoneurons showed significantly lower values (*t* tests, $p < 0.001$ for ***E–G***, asterisks). Scale bars: 500 µm (***A***) and 200 µm (in ***D*** for ***B–D***).

Similar results were obtained with the inhibitory synaptic marker VGAT. As can be appreciated in Figure 5*F*,*G*, SIF motoneurons showed a higher density of VGAT-IR boutons contacting their soma than MIF motoneurons. The location within the oculomotor nucleus of the SIF and MIF motoneurons illustrated in Figure 5*F*,*G*, respectively, is indicated by white arrows in Figure 5*E*. Our measurements showed that MIF ($n = 61$) motoneurons presented a significantly lower VGAT-IR coverage when compared with SIF ($n = 198$) motoneurons (17.17 ± 0.63% and 29.53 ± 0.41%, respectively; *t* test, $t_{(257)} = -15.076$, $p < 0.001$, $d = -2.208$; Fig. 5*H*).

The balance inhibitory-to-total synaptic boutons was estimated as the linear density of VGAT-IR terminals (i.e., inhibitory) with respect to the total linear density of synaptophysin-IR boutons (i.e., excitatory and inhibitory), for both SIF and MIF motoneurons in each animal ($n = 3$). The statistical comparison between MIF and SIF motoneurons revealed no significant difference in the inhibitory-to-total synaptic coverage (Mann–Whitney rank-sum test, $U = 2.000$, $p = 0.400$, $d = 0.995$).

Discussion

We demonstrate for the first time that electrophysiologically-identified MIF and SIF medial rectus motoneurons discharge during slow and fast eye movements. However, MIF motoneurons fired at lower rates, had lower recruitment thresholds, and lower EP and EV sensitivities during spontaneous and vestibular eye movements. A size-principle-based recruitment order was present in both motoneuronal populations. PSTHs obtained following stimulation to the myotendinous junction, where palisade endings are located, revealed no change in the discharge probability of MIF and SIF motoneurons. Finally, MIF motoneurons were also smaller in size, presenting longer antidromic latencies, and lower synaptic coverage.

MIF medial rectus motoneurons discharge during different types of eye movements but with a distinct contribution

The present results show that MIF (and SIF) motoneurons fired during eye fixations, saccades, the slow and fast phases of the vestibulo-ocular reflex and convergent eye movements. These data indicated there are no motoneurons (SIF or MIF) exclusive of certain eye movement type as previously suggested (Wasicky et al., 2004; Ugolini et al., 2006; Bohlen et al., 2017a,b). In line with our findings, all reports on extraocular motoneurons recorded in different vertebrate species, including monkeys, cats, rabbits and fish, have shown that all motoneurons display a tonic-phasic discharge pattern and participate in all types of eye movements (Robinson, 1970; Schiller, 1970; Fuchs and Luschei, 1971; Delgado-Garcia et al., 1986; de la Cruz et al., 1989; Evinger and Baker, 1991; Pastor et al., 1991; Stahl and Simpson, 1995; Davis-López de Carrizosa et al., 2011; Hernández et al., 2017). However, a full exploration of frequencies and amplitudes of stimulation is required to further ascertain the differences in the dynamics of MIF and SIF motoneurons. The vestibulo-ocular pathways manifest differential adaptation properties based on their frequency selectivity (Lisberger et al., 1983), thus it is possible that these separate channels (i.e., low vs high frequency) extend to the motoneurons (Dietrich et al., 2017) and that intrinsic membrane properties along vestibular neurons and motoneurons are tuned to determine the firing and discharge properties of MIF and SIF motoneurons (Serafin et al., 1991a,b; Nieto-Gonzalez et al., 2007; Mayadali et al., 2021). Altogether, it can be suggested that individual extraocular motoneurons do not specialize in producing selectively any of the different types of eye movements (see, however, Henn and Cohen, 1972).

Nonetheless, the present data demonstrated significant differences in several physiological parameters between MIF and SIF medial rectus motoneurons. In general, MIF motoneurons fired at lower frequencies and showed lower EP and EV sensitivities during spontaneous and vestibularly-induced eye movements. Another important finding was that MIF motoneurons were recruited first, as they presented lower thresholds, i.e., EPs more in the off-direction, where small muscle tension is required. As the eye moved toward positions attained in the on-direction they continued firing at increasingly higher rates but still at lower frequencies as compared with SIF motoneurons. This indicates that SIF motoneurons would contribute with higher frequencies at EPs where more tension is required, and therefore, the contribution of MIF and SIF motoneurons throughout the oculomotor range would be different. MIF motoneurons would contribute with low discharge generating small muscle forces and activating first in the off-oculomotor field, whereas SIF motoneurons would contribute with higher FRs to impulse more force for those EPs more in the on-direction.

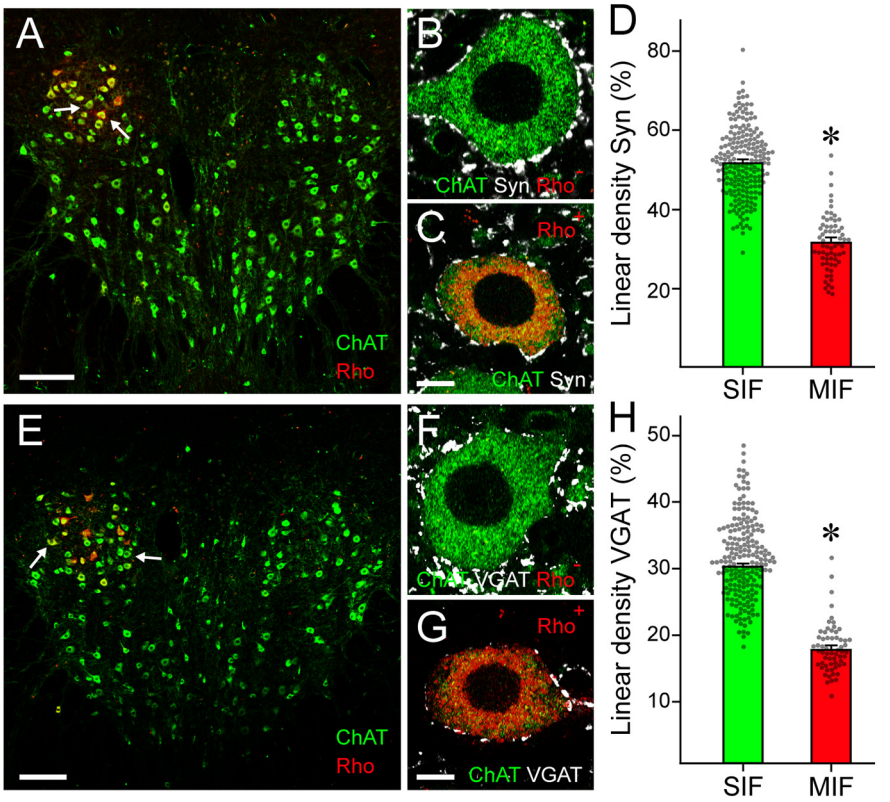

Figure 5. Synaptic coverage of MIF and SIF medial rectus motoneurons. ***A***, Confocal image of the oculomotor nucleus illustrating rhodamine-positive (Rho) MIF motoneurons along with SIF motoneurons, both ChAT-IR. ***B***, ***C***, Synaptophysin labeling (Syn; pseudocolored in white) around the cell body of a medial rectus SIF (***B***, rhodamine-negative and ChAT-positive) and a MIF (***C***, rhodamine-positive and ChAT-positive) motoneuron. These two cells correspond to those indicated by white arrows in ***A***. ***D***, Bar chart illustrating the percentage of the somatic perimeter surrounded by synaptophysin-IR boutons in MIF and SIF medial rectus motoneurons (i.e., linear density, in %). MIF motoneurons received a significantly lower percentage of synaptophysin-IR boutons (asterisk) than SIF motoneurons (*t* test; $p < 0.001$; $n = 206$ SIF and 65 MIF motoneurons). ***E***, Confocal image of the oculomotor nucleus after ChAT immunostaining (in green) and the unilateral injection of rhodamine (in red) in the myotendinous junction of medial rectus muscle. ***F***, ***G***, Examples of a SIF (***F***, rhodamine-negative, ChAT-positive) and a MIF (***G***, rhodamine-positive and ChAT-positive) medial rectus motoneuron after VGAT immunoreactivity (pseudocolored in white). These two motoneurons correspond to the ones pointed by an arrow in ***E***. ***H***, Percentage of the somatic perimeter covered by VGAT-IR boutons (i.e., linear density) around the soma of SIF and MIF motoneurons. MIF motoneurons received a significantly lower percentage of VGAT-IR boutons (asterisk) as compared with SIF motoneurons (*t* test; $p < 0.001$; $n = 198$ SIF and 61 MIF motoneurons). Scale bars: 200 μm (***A***, ***E***), 20 μm (in ***C*** for ***B***, ***C***) and 20 μm (in ***G*** for ***F***, ***G***).

MIF and SIF medial rectus motoneurons display convergent signals

The majority of MIF and SIF medial rectus motoneurons had appropriate signals during spontaneous convergent eye movements, i.e., a small increase in FR. These findings are quite different to those previously reported for cat abducens motoneurons, where most MIF and SIF motoneurons do not exhibit an appropriate response during divergences, but instead a variety of discharge patterns. Thus, a high percentage of MIF and SIF abducens motoneurons either discharged inappropriately, or did not respond, or responded in a variable way to divergences (Hernández et al., 2019).

This discrepancy can be explained considering previous findings of neurons located dorsal and lateral to the oculomotor nucleus that increase their FR with increases in the angle of ocular convergence and that project on medial rectus motoneurons. The output of these so-called midbrain near response cells that might provide the appropriate vergence command needed by the

medial rectus motoneurons (Zhang et al., 1992). In contrast, no divergent gaze signal has been reported to drive abducens motoneurons during disjunctive eye movements so far (Clendaniel and Mays, 1994).

MIF motoneurons have smaller size and receive fewer synaptic boutons

MIF medial rectus motoneurons showed significantly smaller size than SIF medial rectus motoneurons, in agreement with previous reports in monkeys and rats (Eberhorn et al., 2005, 2006). In analogy, previous reports describe that MIF axons are smaller than SIF axons (Mayr, 1971; Browne, 1976; Nelson et al.,1986). The percentage of MIF motoneurons with respect to the total population constituted ~20%, which is also in congruence with previous studies (Büttner-Ennever et al., 2001; Wasicky et al., 2004; Spencer and Porter, 2006; Erichsen et al., 2014; Bohlen et al., 2017b). The smaller size of MIF motoneurons could explain their longer antidromic latencies, and consequently, their expected lower conduction velocity. Similarly, MIF motoneurons of the cat abducens nucleus are smaller and have higher antidromic latencies as compared with SIF abducens motoneurons (Hernández et al., 2019). The finding that MIF motoneurons had smaller size could also correlate with their lower EP threshold, since a small cell responds to a given amount of current with higher excitability, because of its higher input resistance, and therefore, it is recruited first according to the size principle (Henneman et al., 1965).

As demonstrated by synaptophysin immunoreactivity, MIF motoneurons received less synaptic boutons than SIF motoneurons, in agreement with a previous study in monkey medial rectus motoneurons (Erichsen et al., 2014). The smaller density of afferent synaptic boutons driving MIF motoneurons could correlate with their lower FR and sensitivities. The ratio between inhibitory terminals (VGAT-positive) versus the total number of boutons (synaptophysin-positive) was the same for MIF and SIF motoneurons, as happens in the cat abducens nucleus (Hernández et al., 2019).

Relationship between MIF motoneurons and palisade endings

Palisade endings are terminal varicosities at the myotendinous junction around single muscle fiber tips. The muscle fibers associated with palisade endings are the MIFs of the global layer of extraocular muscles, which are characterized by the presence of en grappe nerve endings along their length (Ruskell, 1978; Alvarado-Mallart and Pinçon-Raymond, 1979). We have previously shown that palisade endings are in continuity with MIF motoneuronal axons (Zimmermann et al., 2013; Blumer et al., 2020), thereby en grappe terminals and palisade endings arise both from the same MIF motoneuron. Other authors, however, have hypothesized that palisade endings arise from sensory neurons located in the oculomotor nucleus, which in turn would synapse with MIF motoneurons, suggesting in this way a proprioceptive reflex (Lienbacher and Horn, 2012).

To evaluate this hypothesis, we conducted PSTHs after electrical stimulation to the myotendinous junction while recording the spontaneous discharge of a MIF (or a SIF) motoneurons. It is important to mention that medial rectus muscle in the cat, and in all species studied so far, is the extraocular rectus muscle containing the highest number of palisade endings (Blumer et al., 2016). PSTH analysis revealed no change in the probability of discharge of either MIF or SIF motoneurons, which indicated that the stimulation of palisade endings did not produce any increase or decrease in motoneuronal firing. Therefore, our data indicate that it is unlikely that any signal arrives to motoneurons arising from palisade endings through sensory oculomotor neurons.

An interesting possibility on the functional role of palisade endings and their associated MIF motoneurons (Lienbacher and Horn, 2012; Hoh, 2021) would be that palisade endings, which are in a good location to sense muscle tension, might be activated by muscle stretching during an eye movement and the generated signal would electrically reach their associated en grappe terminals, which in turn would act on the non-twitch muscle fibers, thereby generating a local reflex (Lienbacher and Horn, 2012; Hoh, 2021). Since palisade endings have been described displaying motor (Konakci et al., 2005; Blumer et al., 2009; Rungaldier et al., 2009; Zimmermann et al., 2013) and sensory (Ruskell, 1978; Alvarado-Mallart and Pinçon-Raymond, 1979; Billig et al., 1997; Büttner-Ennever et al., 2003; Lienbacher et al., 2011) characteristics, the hypothesis of an intrinsic sensory-motor reflex seems to reconcile all data (Hoh, 2021).

New perspectives arise in motor control with the tandem of MIF and palisade endings. If palisade endings were proprioceptive organs originating from MIF motoneurons, the possibility of an intrinsic local reflex between palisade endings and en passant boutons of MIF in the muscle is an attractive hypothesis to be studied in the near future. It is clear that proprioception in extraocular muscles would open a new vision beyond the classic proprioception in skeletal muscle. Moreover, the significance of heterogeneity of motoneuron pools, as shown in here, is a crucial question for motor control.

References

Akagi Y (1978) The localization of the motor neurons innervating the extraocular muscles in the oculomotor nuclei of the cat and rabbit, using horseradish peroxidase. J Comp Neurol 181:745–761.

Alvarado-Mallart RM, Pinçon-Raymond M (1979) The palisade endings of cat extraocular muscles: a light and electron microscope study. Tissue Cell 11:567–584.

Bach-y-Rita P, Ito F (1966) In vivo studies on fast and slow muscle fibers in cat extraocular muscles. J Gen Physiol 49:1177–1198.

Billig I, Buisseret Delmas C, Buisseret P (1997) Identification of nerve endings in cat extraocular muscles. Anat Rec 248:566–575.

Blumer R, Konakci KZ, Pomikal C, Wieczorek G, Lukas JR, Streicher J (2009) Palisade endings: cholinergic sensory organs or effector organs? Invest Ophthalmol Vis Sci 50:1176–1186.

Blumer R, Maurer-Gesek B, Gesslbauer B, Blumer M, Pechriggl E, Davis-López de Carrizosa MA, Horn AK, May PJ, Streicher J, de la Cruz RR, Pastor AM (2016) Palisade endings are a constant feature in the extraocular muscles of frontal-eyed, but not lateral-eyed, animals. Invest Ophthalmol Vis Sci 57:320–331.

Blumer R, Streicher J, Davis-López de Carrizosa MA, de la Cruz RR, Pastor AM (2017) Palisade endings of extraocular muscles develop postnatally following different time courses. Invest Ophthalmol Vis Sci 58:5105–5121.

Blumer R, Streicher J, Carrero-Rojas G, Calvo PM, de la Cruz RR, Pastor AM (2020) Palisade endings have an exocytotic machinery but lack acetylcholine receptors and distinct acetylcholinesterase activity. Invest Ophthalmol Vis Sci 61:31.

Bohlen MO, Warren S, May PJ (2017a) A central mesencephalic reticular formation projection to medial rectus motoneurons supplying singly and multiply innervated extraocular muscle fibers. J Comp Neurol 525:2000–2018.

Bohlen MO, Warren S, Mustari MJ, May PJ (2017b) Examination of feline extraocular motoneuron pools as a function of muscle fiber innervation type and muscle layer. J Comp Neurol 525:919–935.

Bondi AY, Chiarandini DJ (1983) Morphologic and electrophysiologic identification of multiply innervated fibers in rat extraocular muscles. Invest Ophthalmol Vis Sci 24:516–519.

Browne JS (1976) The contractile properties of slow muscle fibres in sheep extraocular muscle. J Physiol 254:535–550.

Büttner-Ennever JA (2006) The extraocular motor nuclei: organization and functional neuroanatomy. In: Neuroanatomy of the oculomotor system (Büttner-Ennever JA, ed), pp 95–125. San Diego: Elsevier.

Büttner-Ennever JA, Horn AKE (2002) The neuroanatomical basis of oculomotor disorders: the dual motor control of extraocular muscles and its possible role in proprioception. Curr Opin Neurol 15:35–43.

Büttner-Ennever JA, Horn AK, Scherberger H, D'Ascanio P (2001) Motoneurons of twitch and nontwitch extraocular muscle fibers in the abducens, trochlear, and oculomotor nuclei of monkeys. J Comp Neurol 438:318–335.

Büttner-Ennever JA, Eberhorn A, Horn AKE (2003) Motor and sensory innervation of extraocular eye muscles. Ann NY Acad Sci 1004: 40–49.

Clendaniel RA, Mays LE (1994) Characteristics of antidromically identified oculomotor internuclear neurons during vergence and versional eye movements. J Neurophysiol 71:1111–1127.

Davis-López de Carrizosa MA, Morado-Díaz CJ, Miller JM, de la Cruz RR, Pastor AM (2011) Dual encoding of muscle tension and eye position by abducens motoneurons. J Neurosci 31:2271–2279.

Davis-López de Carrizosa MA, Morado-Díaz CJ, Tena JJ, Benítez-Temiño B, Pecero ML, Morcuende SR, de la Cruz RR, Pastor AM (2009) Complementary actions of BDNF and neurotrophin-3 on the firing patterns and synaptic composition of motoneurons. J Neurosci 29:575–587.

de la Cruz RR, Escudero M, Delgado-García JM (1989) Behaviour of medial rectus motoneurons in the alert cat. Eur J Neurosci 1:288–295.

de la Cruz RR, Pastor AM, Delgado-García JM (1994) Effects of target depletion on adult mammalian central neurons: morphological correlates. Neuroscience 58:59–79.

Delgado-Garcia JM, del Pozo F, Baker R (1986) Behavior of neurons in the abducens nucleus of the alert cat-I. Motoneurons. Neuroscience 17:929–952.

Dietrich H, Glasauer S, Straka H (2017) Functional organization of vestibulo-ocular responses in abducens motoneurons. J Neurosci 37:4032–4045.

Eberhorn AC, Ardeleanu P, Büttner-Ennever JA, Horn AKE (2005) Histochemical differences between motoneurons supplying multiply and singly innervated extraocular muscle fibers. J Comp Neurol 491:352–366.

Eberhorn AC, Büttner-Ennever JA, Horn AKE (2006) Identification of motoneurons supplying multiply- or singly-innervated extraocular muscle fibers in the rat. Neuroscience 137:891–903.

Eladly A, Del Valle J, Minguillon J, Mercadal B, Becerra-Fajardo L, Navarro X, Ivorra A (2020) Interleaved intramuscular stimulation with minimally overlapping electrodes evokes smooth and fatigue resistant forces. J Neural Eng 17:046037.

Enoka RM, Amiridis IG, Duchateau J (2020) Electrical stimulation of muscle: electrophysiology and rehabilitation. Physiology (Bethesda) 35:40–56.

Erichsen JT, Wright NF, May PJ (2014) Morphology and ultrastructure of medial rectus subgroup motoneurons in the macaque monkey. J Comp Neurol 522:626–641.

Evinger C, Baker R (1991) Are there subdivisions of extraocular motoneuronal pools that can be controlled selectively? In Motor control: concepts and issues (Humphrey DR, Freund HJ, eds), pp 23–31. Hoboken: Wiley Ltd.

Fuchs AF, Luschei ES (1971) The activity of single trochlear nerve fibers during eye movements in the alert monkey. Exp Brain Res 13:78–89.

Fuchs AF, Robinson DA (1966) A method for measuring horizontal and vertical eye movement chronically in the monkey. J Appl Physiol 21:1068–1070.

Fuchs AF, Scudder CA, Kaneko CR (1988) Discharge patterns and recruitment order of identified motoneurons and internuclear neurons in the monkey abducens nucleus. J Neurophysiol 60:1874–1895.

Henn V, Cohen B (1972) Eye muscle motor neurons with different functional characteristics. Brain Res 45:561–568.

Henneman E, Somjen G, Carpenter DO (1965) Functional significance of cell size in spinal motoneurons. J Neurophysiol 28:560–580.

Hernández RG, Benítez-Temiño B, Morado-Díaz CJ, Davis-López de Carrizosa MA, de la Cruz RR, Pastor AM (2017) Effects of selective deafferentation on the discharge characteristics of medial rectus motoneurons. J Neurosci 37:9172–9188.

Hernández RG, Calvo PM, Blumer R, de la Cruz RR, Pastor AM (2019) Functional diversity of motoneurons in the oculomotor system. Proc Natl Acad Sci USA 116:3837–3846.

Hess A, Pilar G (1963) Slow fibres in the extraocular muscles of the cat. J Physiol 169:780–798.

Hoh JFY (2021) Myosin heavy chains in extraocular muscle fibres: distribution, regulation and function. Acta Physiol (Oxf) 231:e13535.

Horn AKE, Horng A, Buresch N, Messoudi A, Härtig W (2018) Identification of functional cell groups in the abducens nucleus of monkey and human by perineuronal nets and choline acetyltransferase immunolabeling. Front Neuroanat 12:45.

Konakci KZ, Streicher J, Hoetzenecker W, Blumer MJF, Lukas JR, Blumer R (2005) Molecular characteristics suggest an effector function of palisade endings in extraocular muscles. Invest Ophthalmol Vis Sci 46:155–165.

Lienbacher K, Horn AKE (2012) Palisade endings and proprioception in extraocular muscles: a comparison with skeletal muscles. Biol Cybern 106:643–655.

Lienbacher K, Mustari M, Ying HS, Büttner-Ennever JA, Horn AKE (2011) Do palisade endings in extraocular muscles arise from neurons in the motor nuclei? Invest Ophthalmol Vis Sci 52:2510–2519.

Lisberger SG, Miles FA, Optican LM (1983) Frequency-selective adaptation: evidence for channels in the vestibulo-ocular reflex? J Neurosci 3:1234–1244.

Mayadali ÛS, Fleuriet J, Mustari M, Straka H, Horn AKE (2021) Transmitter and ion channel profiles of neurons in the primate abducens and trochlear nuclei. Brain Struct Funct 226:2125–2151.

Mayr R (1971) Structure and distribution of fibre types in the external eye muscles of the rat. Tissue Cell 3:433–462.

Miyazaki S (1985) Location of motoneurons in the oculomotor nucleus and the course of their axons in the oculomotor nerve. Brain Res 348:57–63.

Namba T, Nakamura T, Takahashi A, Grob D (1968) Motor nerve endings in extraocular muscles. J Comp Neurol 134:385–396.

Nelson JS, Goldberg SJ, McClung JR (1986) Motoneuron electrophysiological and muscle contractile properties of superior oblique motor units in cat. J Neurophysiol 55:715–726.

Nieto-Gonzalez JL, Carrascal L, Nunez-Abades P, Torres B (2007) Phasic and tonic firing properties in rat oculomotor nucleus motoneurons, studied in vitro. Eur J Neurosci 25:2682–2696.

Pastor AM, González-Forero D (2003) Recruitment order of cat abducens motoneurons and internuclear neurons. J Neurophysiol 90:2240–2252.

Pastor AM, Torres B, Delgado-García JM, Baker R (1991) Discharge characteristics of medial rectus and abducens motoneurons in the goldfish. J Neurophysiol 66:2125–2140.

Pilar G (1967) Further study of the electrical and machanical responses of slow fibers in cat extraocular muscles. J Gen Physiol 50:2289–2300.

Robinson DA (1970) Oculomotor unit behavior in the monkey. J Neurophysiol 33:393–403.

Rungaldier S, Pomikal C, Streicher J, Blumer R (2009) Palisade endings are present in canine extraocular muscles and have a cholinergic phenotype. Neurosci Lett 465:199–203.

Ruskell GL (1978) The fine structure of innervated myotendinous cylinders in extraocular muscles of rhesus monkeys. J Neurocytol 7:693–708.

Schiaffino S, Reggiani C (2011) Fiber types in mammalian skeletal muscles. Physiol Rev 91:1447–1531.

Schiller PH (1970) The discharge characteristics of single units in the oculomotor and abducens nuclei of the unanesthetized monkey. Exp Brain Res 10:347–362.

Serafin M, de Waele C, Khateb A, Vidal PP, Mühlethaler M (1991a) Medial vestibular nucleus in the guinea-pig. I. Intrinsic membrane properties in brainstem slices. Exp Brain Res 84:417–425.

Serafin M, de Waele C, Khateb A, Vidal PP, Mühlethaler M (1991b) Medial vestibular nucleus in the guinea-pig. II. Ionic basis of the intrinsic membrane properties in brainstem slices. Exp Brain Res 84:426–433.

Shall MS, Goldberg SJ (1992) Extraocular motor units: type classification and motoneuron stimulation frequency-muscle unit force relationships. Brain Res 587:291–300.

Spencer RF, Porter JD (2006) Biological organization of the extraocular muscles. Prog Brain Res 151:43–80.

Stahl JS, Simpson JI (1995) Dynamics of abducens nucleus neurons in the awake rabbit. J Neurophysiol 73:1383–1395.

Tang X, Büttner-Ennever JA, Mustari MJ, Horn AKE (2015) Internal organization of medial rectus and inferior rectus muscle neurons in the C group of the oculomotor nucleus in monkey. J Comp Neurol 523:1809–1823.

Ugolini G, Klam F, Doldan Dans M, Dubayle D, Brandi AM, Büttner-Ennever J, Graf W (2006) Horizontal eye movement networks in primates as revealed by retrograde transneuronal transfer of rabies virus: differences in monosynaptic input to "slow" and "fast" abducens motoneurons. J Comp Neurol 498:762–785.

Wasicky R, Horn AKE, Büttner-Ennever JA (2004) Twitch and non-twitch motoneuron subgroups in the oculomotor nucleus of monkeys receive different afferent projections. J Comp Neurol 479:117–129.

Zhang Y, Mays LE, Gamlin PD (1992) Characteristics of near response cells projecting to the oculomotor nucleus. J Neurophysiol 67:944–960.

Zimmermann L, Morado-Díaz CJ, Davis-López de Carrizosa MA, de la Cruz RR, May PJ, Streicher J, Pastor AM, Blumer R (2013) Axons giving rise to the palisade endings of feline extraocular muscles display motor features. J Neurosci 33:2784–2793.